Received March 2003
Revised November 2003
Accepted December 2003

Finite volume approach for solving multiphase flows in vertical pneumatic dryers

I. Skuratovsky and A. Levy
Mechanical Engineering Department, Pearlstone Center for Aeronautical Engineering Studies, Ben-Gurion University of the Negev, Beer-Sheva, Israel

Keywords *Flow, Heat transfer, Mass transfer, Numerical analysis, Finite volume methods*

Abstract *In the present study, a finite volume approach for solving two-dimensional, two-fluids flows with heat and mass transfer was developed for predicting the flow of particulate materials through pneumatic dryer. The model was solved for a two-dimensional steady-state condition and considering axial and radial profiles for the flow variables. A two-stage drying process was implemented. The numerical procedure includes discretization of calculation domain into torus-shaped final volumes, solving the gas phase conservation equations by a modified semi-implicit method for pressure-linked equations algorithm, and the conservation equations of particulate phase were solved by the explicit forward difference algorithm. The mass momentum and energy coupling between the phases were considered by principles of the Interphase slip algorithm. In order to validate the theoretical and the numerical models, the developed models were applied to simulate the drying process of wet PVC particles in a large-scale pneumatic dryer and to the drying process of wet sand in a laboratory-scale pneumatic dryer. The predictions of the numerical simulations were compared successfully with the results of independent numerical and experimental investigations. Following the models validation, the two-dimensional distributions of the flow characteristics were examined.*

Notation

A = area (m^2)
a = coefficient in the discretization equation
b = constant term in the discretization equation
c = specific heat (J/kg K)
c_p = specific heat at constant pressure (J/kg K)
C_d = drag coefficient
C_{vm} = virtual mass coefficient
d = coefficient of the pressure difference term
D = diffusion conductance at cell face (kg/m^2s)
D_p = particle diameter (m)
D_i = diameter of the wet core particle (m)
D_o = dry crust diameter (m)
D_v = diffusion coefficient of water vapor in air within a pore (m^2/s)
F = convective mass flux per unit area (kg/m^2s)
F_α = force per unit volume of the α-phase (N/m^3)
g = gravity acceleration (m/s^2)
H_α = enthalpy of the α-phase (J/kg)
H_{gd} = enthalpy of the water vapor (J/kg)
h = heat transfer coefficient (W/m^2K)
h_d = convective mass transfer coefficient (m/s)
k = thermal conductivity (W/mK)
M = molecular weight (kg/kmole)
M_{H_2O} = molecular weight of water (kg/kmole)
N_d = number of particles per unit volume (m^{-3})
Nu = Nusselt number
m = mass (ng)
$\dot{m}_d$ = evaporation rate, from a single particle (kg/s)

International Journal of Numerical Methods for Heat & Fluid Flow
Vol. 14 No. 8, 2004
pp. 980-1001

0961-5539
DOI 10.1108/09615530410546290

p = pressure (Pa)
p_v = partial pressure of water vapor (Pa)
Pr = Prandtl number
Q_α = heat transfer between the phases per unit volume (W/m^3)
$\mathscr{R}$ = gas constant (J/kg K)
Re = Reynolds number
Sc = Schmidt number
S_m = mass transfer per unit length (kg/ms)
Sh = Sherwood number
T_α = temperature of the α-phase (K)
T_s = crust temperature (K)
T_{wall} = pipe wall's temperature (K)
T_{ave} = average temperature [$\equiv 0.5(T_s + T_d)$] (K)
u_r = ($\equiv u_g - u_d$) relative velocity between the phases (m/s)
u_α = velocity of the α-phase (m/s)
V = volume (m^3)
W_α = work per unit length done between the phases (W/m)
X_w = water vapor mass concentration in the gas phase
Y_w = molar concentration of water vapor in the gas phase

Greek Symbols

ε = void fraction of the particle (porosity)
μ_g = gas dynamic viscosity
ρ_α = density of the α-phase
$\rho_{v\alpha}$ = water vapor density at the α-phase
ρ = density
ξ = water concentration in the particle
ϕ_α = volume fraction of the α-phase
φ = dummy property

Subscripts

d = the dispersed phase
da = dry air properties
e = east face of the control volume
g = the gas phase
n = north face of the control volume
sat = saturation
s = solid properties or south face of the control volume
v = vapor properties
w = water properties or west face of the control volume
wa = water properties in air
wd = water properties in dispersed phase

Introduction

Generally, three types of theoretical approaches can be used for modeling the gas-particles flows in the pneumatic dryers, namely, Two-fluid Theory (Bowen, 1976), Eulerian Granular (Gidaspow, 1994) and the Discrete Element Method (Cundall and Strack, 1979). Traditionally, the Two-fluid Model was used to describe a dilute phase flow. In dilute phase flow, particle-particle and particle-wall interactions are usually being neglected (Crowe, 1982). The theory is based on macroscopic balance equations of mass, momentum and energy for both the gas and the solid phases. The model treated the dispersed phase, i.e. the solid phase as a pseudo-fluid and assumed that both phases are occupying every point of the computational domain with its own volume fraction. Often, the flow in a pneumatic dryer can be classified as dilute phase flow and, therefore, it was decided to adopt this method in this study.

A wide spread approach to predict the drying process is based on a steady state one-dimensional mathematical formulation of the conservation equations. Using this approach one can predict the average values of various properties of the phases in cross sections of the dryer (Andrieu and Bressat, 1982; Baeyens *et al.*, 1995; Levi-Hevroni *et al.*, 1995; Levy and Borde, 1999; Levy *et al.*, 1988; Mindziul and Kmiec, 1996 and Rocha and Paixão, 1996).

In contrast to traditional one-dimensional models, in the present study, the two-dimensional pneumatic drying model of Skuratovsky *et al.* (2003) was adopted. The model is based on the Two-fluid Eulerian theory and was used to describe the steady state, two-dimensional dilute phase flow of a wet dispersed phase (wet solid particles) in a continuous gas phase through a pneumatic dryer.

In order to validate the numerical model, the predictions of the numerical solutions were compared with the results of other one-dimensional numerical solutions and experimental data of Baeyens *et al.* (1995) and Rocha (1988). In addition, the axial and the radial distributions of the characteristic properties were examined.

The present study

Owing to the fact that detailed derivations of the governing equations can be found in Skuratovsky *et al.* (2003), in the following, only the final form of the two-dimensional governing equations and the assumptions on which their derivation was based are presented.

The pneumatic drying model is based on the following assumptions.

- The gas behaves as an ideal gas.
- Steady-state flow.
- The gas phase is a mixture of water vapor with air.
- Influence of gravity on gas phase is neglected.
- Dispersed phase behavior id like continuous phase behavior.
- The particles are made from a substance containing a solid porous matrix and liquid or gas with liquid-vapor.
- At the first drying stage, the particle is isothermal and at the second drying stage the particle wet core temperature is different from that of dry crust.
- The specific densities of the liquid and the solid, which compose the particle, are constants.
- The influence of the pressure gradient on the inertia of the solid particles is negligible in comparison to that of the drag force.
- Mass, momentum and heat transfer occur only between the two phases and not between the particles themselves.
- Heat transfer can occur between the pipe wall and the continuous gas phase.
- Conductive heat flux is negligibly small in comparison with the convective heat flux in the Z direction.
- The flow in the dryer is vertical, two-dimensional, non-rotational and axisymmetrical.
- Non-slip and non-penetrating wall conditions.
- Electrical and surface tension forces are neglected.

It should be pointed out here that based on the assumption that the two-dimensional vertical flow is non-rotational and axisymmetrical both phases' velocities have only one component, which is in the Z direction and they are a function of both the axial and the radial location in the pipe. Based on the above-mentioned assumptions the conservation equations of the gas and the solid phases were written.

- Mass balance of the gas-phase

$$\frac{\partial(\rho_g u_g \phi_g)}{\partial z} = S_m \tag{1}$$

- Momentum balance of the gas-phase

In dilute phase flow, the cross sectional area of the particles in the pipe is usually small, and therefore, the influence of the pressure gradient on the inertia of the solid particles is negligible in comparison to that of the drag force. Hence, it was assumed that the pressure gradient contributes only to the momentum of the gas phase.

$$\frac{\partial\left(\rho_g u_g^2 \phi_g\right)}{\partial z} = -\frac{\partial P}{\partial z} + \left[\frac{1}{r}\frac{\partial}{\partial r}\left(r\phi_g \mu_g \frac{\partial u_g}{\partial r}\right)\right] + F_g + S_m u_d + \frac{\partial}{\partial z}\left(\phi_g \mu_g \frac{\partial u_g}{\partial z}\right) \quad (2)$$

- Energy balance equations of the gas phase

$$\frac{\partial}{\partial z}\left[\phi_g \rho_g u_g\left(H_g + \frac{u_g^2}{2}\right)\right] = \frac{1}{r}\frac{\partial}{\partial r}\left(\phi_g k_g r \frac{\partial T_g}{\partial r}\right) + Q_g - W_g + S_m\left(H_{gd} + \frac{u_d^2}{2}\right) \quad (3)$$

- Mass balance of the dispersed phase

$$\frac{\partial(\rho_d u_d \phi_d)}{\partial z} = -S_m \quad (4)$$

- Momentum balance equation of dispersed phase

$$\frac{\partial\left(\rho_d u_d^2 \phi_d\right)}{\partial z} = -\rho_d g \phi_d + F_d - S_m u_d \quad (5)$$

- Energy balance equations for dispersed phase

$$\frac{\partial}{\partial z}\left[\phi_d \rho_d u_d\left(H_d + \frac{u_d^2}{2}\right)\right] = Q_d - W_d - \rho_d u_d \phi_d g - S_m\left(H_{gd} + \frac{u_d^2}{2}\right) \quad (6)$$

Subtracting the momentum balance equation of the dispersed phase (equation (5)) multiplied by the dispersed phase velocity from it's energy balance equation results in

$$\frac{\partial}{\partial z}[\phi_d \rho_d u_d c_s T_d] = Q_d - S_m H_{gd} \quad (7)$$

Complimentary equations

In order to solve the above set of differential equations, several complimentary equations, definitions and empirical correlations are required. These will be presented subsequently. It should also be noted that both the gas and the dispersed phases are mixtures and hence all their thermodynamics properties were calculated using the mixture theory.

- The volume fraction definition and equation

$$\phi_g = \frac{V_g}{V}; \quad \phi_d = \frac{V_d}{V}; \quad \phi_g + \phi_d = 1 \quad (8)$$

- Drag forces

The acting forces per unit volume between the phases that were taken into account were due to drag and virtual-mass.

$$F_{\mathrm{d}} = -F_{\mathrm{g}} = N_{\mathrm{d}}\rho_{\mathrm{g}}\left[C_{\mathrm{d}}\frac{\pi D_{\mathrm{p}}^2}{4}\frac{1}{2}u_{\mathrm{r}}|u_{\mathrm{r}}| + c_{\mathrm{vm}}\frac{\pi D_{\mathrm{p}}^3}{6}u_{\mathrm{d}}\frac{\mathrm{d}u_{\mathrm{r}}}{\mathrm{d}z}\right] \tag{9}$$

where the number of the particles per unit volume, N_{d}, was expressed by

$$N_{\mathrm{d}} = \frac{6\phi_{\mathrm{d}}}{\pi D_{\mathrm{p}}^3} \tag{10}$$

The drag coefficient, C_{d}, was calculated via the correlations that have been presented by Ossen *et al.* and can be found in Clift *et al.* (1987).

$$\begin{aligned}
&C_{\mathrm{d}} = \frac{64}{\pi\mathrm{Re}}\left(1 + \frac{\mathrm{Re}}{2\pi}\right) \quad \text{for } \mathrm{Re} < 0.01\\
&C_{\mathrm{d}} = \frac{64}{\pi\mathrm{Re}}(1 + 10^{x}) \quad \text{for } 0.01 < \mathrm{Re} < 1.5\\
&x = -0883 + 0.906Lg(\mathrm{Re}) - 0.025(Lg(\mathrm{Re}))^2\\
&C_{\mathrm{d}} = \frac{64}{\pi\mathrm{Re}}(1 + 0.138\mathrm{Re}^{0.792}) \quad \text{for } 1.5 < \mathrm{Re} < 133\\
&Lg(C_{\mathrm{d}}) = 2.0351 - 1.66Lg(\mathrm{Re}) + Lg^2(\mathrm{Re}) - 0.0306Lg^3(\mathrm{Re})\\
&\qquad\qquad \text{for } 40 < \mathrm{Re} < 1000
\end{aligned} \tag{11}$$

The effective mass of the dispersed phase is usually described by the virtual-mass coefficient, C_{vm}. In general, this coefficient is a function of the volume fraction of the dispersed phase, ϕ_{d}, and the particle shape, but it is often taken as constant. For a rigid spherical particle $C_{\mathrm{vm}} = 0.5$ and this value was used in the course of this work (Clift *et al.*, 1987).

Work and heat transfer

The work acting between the two phases per unit length was written as

$$W_{\mathrm{g}} = -W_{\mathrm{d}} = -F_{\mathrm{g}}u_{\mathrm{d}} = F_{\mathrm{d}}u_{\mathrm{d}} \tag{12}$$

The convective heat transfer between the phases was expressed by

$$Q_{\mathrm{d}} = -Q_{\mathrm{g}} = \frac{6\phi_{\mathrm{d}}}{D_{\mathrm{p}}}h(T_{\mathrm{g}} - T_{\mathrm{s}}) \tag{13}$$

The convective heat transfer coefficient, h, was calculated from the Nusselt number, Nu, which is often expressed as a function of the Reynolds number, Re, and Prandtl number, Pr.

$$\mathrm{Nu} = \frac{hD_\mathrm{p}}{k_\mathrm{g}} = F(\mathrm{Re}, \mathrm{Pr}); \quad \mathrm{Re} = \frac{\rho_\mathrm{g}|u_\mathrm{r}|D_\mathrm{p}}{\mu_\mathrm{g}}; \quad \mathrm{Pr} = \frac{\mu_\mathrm{g}c_\mathrm{pg}}{k_\mathrm{g}} \tag{14}$$

Various empirical correlations may be found in the literature. Baeyens *et al.* (1995) present various empirical correlations that may be used to calculate the heat transfer coefficient, but only two of them, which were originally developed for a pneumatic dryer, yield good agreement with experimental data (Levy and Borde, 1999). In the present study the correlation that was developed by Baeyens *et al.* (1995) for large scale pneumatic dryer was applied.

$$\mathrm{Nu} = 0.15\,\mathrm{Re} \tag{15}$$

During the second drying period, the model assumed that the particle consists of a dry crust surrounding a wet core. Hence, the particle is characterized by two temperatures, i.e. the particle's crust and core temperatures, T_s and T_d, respectively. Furthermore, it was assumed that the heat transfer from the particle's crust to the gas phase is equal to that transferred from the wet core to the gas phase. Thus, the following heat balance equation can be written.

$$(T_\mathrm{g} - T_\mathrm{s})\left(\frac{1}{h\pi D_\mathrm{p}^2}\right)^{-1} = (T_\mathrm{g} - T_\mathrm{d})\left(\frac{1}{h\pi D_\mathrm{p}^2} + \frac{D_\mathrm{p} - D_\mathrm{i}}{2\pi D_\mathrm{p} D_\mathrm{i} k_\mathrm{ps}}\right)^{-1} \tag{16}$$

Mass transfer

The mass transfer source term can be obtained by multiplying the evaporation rate from a single particle, $\dot{m}_\mathrm{d}$, by the total number of particles per unit volume, i.e.

$$S_\mathrm{m} = N_\mathrm{d}\dot{m}_\mathrm{d} \tag{17}$$

In the first drying period, the gas phase resistance controls the evaporation rate. The resistance between the gas and the wet envelope of the wet particle was expressed by

$$\dot{m}_\mathrm{d} = h_\mathrm{d}\pi D_\mathrm{p}^2\left(\frac{M_\mathrm{w}p_\mathrm{vo}}{\mathscr{R}T_\mathrm{s}} - \frac{M_\mathrm{w}p_\mathrm{vg}}{\mathscr{R}T_\mathrm{g}}\right) \tag{18}$$

When the liquid evaporated from the particle surface and it filled all the voids inside the porous particle, the second drying period starts. The critical solid-to-liquid mass ratio, which is obtained from the minimum void fraction, i.e. the porosity of the particles, ε, controls the transfer between drying periods and as a consequence, it controls the mass transfer model that was used. For the purpose of numerical calculation, the model takes a representative value of 0.15 for the particle porosity. During the second period of the drying process, the dry crust causes additional resistance to heat and mass transfer. This resistance is governed by a diffusion process. During this period, the outside diameter of the particle, D_o, is assumed to remain constant and the diameter of the wet core, D_i, decreases. The evaporation rate from a particle with a dry crust can be expressed by Stephan-type diffusion rule (Abuaf and Staub, 1987). Assuming that the mass flow rate of vapor emerging out from the crust is equal to that of the liquid evaporating and diffusing out of the wet core, an implicit equation for calculating the evaporation rate, $\dot{m}_\mathrm{d}$, can be obtained.

$$\dot{m}_{\mathrm{d}} = -\frac{D_{\mathrm{i}} - D_{\mathrm{o}}}{D_{\mathrm{o}} D_{\mathrm{i}}} \frac{2\pi\varepsilon \mathrm{D_v} p}{\mathscr{R} T_{\mathrm{ave}}} \ell \mathrm{n}\left((p - p_{\mathrm{sat}}) / \left(p - \frac{R T_{\mathrm{s}}}{h_{\mathrm{d}} \pi D_{\mathrm{o}}^2 M_{\mathrm{w}}} \dot{m}_{\mathrm{d}} - \frac{p_{\mathrm{vg}} T_{\mathrm{s}}}{T_{\mathrm{g}}} \right) \right) \tag{19}$$

The mass transfer coefficient, h_{d}, was calculated in analogy to the heat transfer coefficient, h, from the Sherwood number, Sh, which is equivalent to the Nusselt number, Nu

$$\mathrm{Sh} = \frac{h_{\mathrm{d}} D_{\mathrm{p}}}{D_{\mathrm{v}}} = F(\mathrm{Re}, \mathrm{Sc}); \quad \mathrm{Sc} = \frac{\mu_{\mathrm{g}}}{\rho_{\mathrm{g}} D_{\mathrm{v}}} \tag{20}$$

Equation (15) was used to calculate the Sherwood number, Sh and the mass transfer coefficient, h_{d} during this study.

Particle diameter

The diameter of the wet particle during the first drying period was calculated by

$$\frac{\mathrm{d}D_{\mathrm{p}}}{\mathrm{d}z} = \frac{2}{u_{\mathrm{d}} \pi D_{\mathrm{p}}^2 \rho_{\mathrm{wd}}} \frac{S_{\mathrm{m}}}{N_{\mathrm{d}}} \tag{21}$$

In general, during the second drying period, the outer shape of particle might be changed due to the shrinkage of both outer and core diameter. However, to simplify the model, it was assumed that the particle outer diameter remains constant during the second drying period. Thus, only the change of the wet core diameter, D_{i}, was considered.

$$\frac{\mathrm{d}D_{\mathrm{i}}}{\mathrm{d}z} = \frac{2}{\varepsilon u_{\mathrm{d}} \pi D_{\mathrm{i}}^2 \rho_{\mathrm{wd}}} \frac{S_{\mathrm{m}}}{N_{\mathrm{d}}} \tag{22}$$

Particle's water concentration

The mass concentration of the water in the particle was defined by

$$\xi = \frac{m_{\mathrm{wd}}}{m_{\mathrm{wd}} + m_{\mathrm{s}}} \tag{23}$$

The change of water mass concentration in the particle along the dryer was described as a function of the mass transfer between the phases as

$$\frac{\mathrm{d}\xi}{\mathrm{d}z} = \frac{6(1 - \xi)}{u_{\mathrm{d}} \rho_{\mathrm{d}} \pi D_{\mathrm{p}}^3} \frac{S_{\mathrm{m}}}{N_{\mathrm{d}}} \tag{24}$$

Particle density

Since the particle is composed of both liquid water and porous solid structure, its density is dependent on the liquid and solid intrinsic densities and on the particle's water concentration.

$$\frac{1}{\rho_{\mathrm{d}}} = \frac{\xi}{\rho_{\mathrm{wd}}} + \frac{(1 - \xi)}{\rho_{\mathrm{s}}} \tag{25}$$

Water vapor diffusion equation and equation of state for the gas phase

The mass and the molecular concentrations of water vapor in the gas phase were defined by

$$X_w = \frac{m_{wa}}{m_g} = \frac{m_{wa}}{m_{da} + m_{wa}} \quad Y_w = \frac{X_w M_{da}}{X_w M_{da} + (1 - X_w) M_{H_2O}} \tag{26}$$

In order to take into consideration the influence of the water vapor on the gas phase density, the molar concentration of the water vapor in the gas phase was used together with the ideal gas equation in the following way

$$R_g = \frac{\mathscr{R}}{M_g}; \quad M_g = Y_w M_{H_2O} + (1 - Y_w) M_{da}; \quad \rho_g = \frac{P}{R_g T_g} \tag{27}$$

The water vapor distribution in the gas phase was calculated by the water vapor diffusion equation.

$$\frac{\partial}{\partial z}(\phi_g \rho_g u_g X_w) = \frac{\partial}{r \partial r}\left(D_v \rho_g \phi_g r \frac{\partial X_w}{\partial r}\right) + \frac{\partial}{\partial z}\left(D_v \rho_g \phi_g \frac{\partial X_w}{\partial z}\right) + S_m \tag{28}$$

Numerical model

The above-mentioned mathematical model cannot be solved by any analytical method. Therefore, it was decided to solve the model numerically. The numerical procedure includes discretization of the calculation domain into torus-shaped final volumes (Figure 1). The gas-phase conservation equations (2), (3) and (28) are a set of parabolic partial differential equations (PDE) and the solid phase balance equations obtained as a set of ordinary differential equations (ODE). Therefore, a splitting technique was applied for solving the two sets of differential equations over the computational domain. The gas phase conservation equations were solved by a modified Semi-implicit method for pressure-linked equations (SIMPLE) algorithm (Patankar, 1980) and the solid phase equations were solved by forward difference approximation. The various coupling terms between both phases were considered by principles of the Interphase slip algorithm (IPSA) (Spalding, 1983).

Generally, calculations of the scalar variables φ (such as, temperatures, densities, etc.) are dependent on the magnitude and direction of the velocity field. To evaluate the

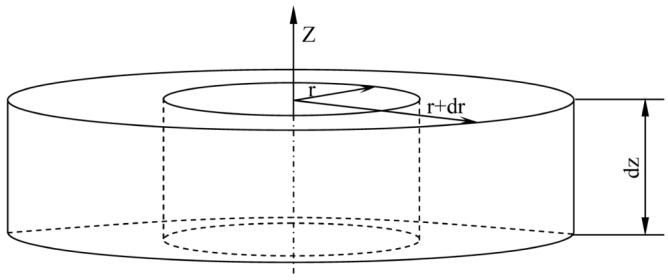

Figure 1.
Typical torus-shaped final volume

velocity field of the gas phase, both momentum and continuity equations need to be solved. The solution of these equations presents three new problems.

- The convective terms of the momentum equation contain non-linear terms, e.g. $\partial(\rho_g u_g^2 \phi_g)/\partial z$.
- Transport equations are intricately coupled with the velocity components.
- Complicated way to evaluate pressure field, evidently no equation for pressure.

If the pressure gradient is known, the process of obtaining discretized equations for the velocity from the momentum equation is similar for any other scalar and will be presented in a following section. The problems associated with the non-linearity in the momentum equation and the pressure-velocity linkage can be resolved by adoption of an iterative solution strategy, such as the SIMPLE algorithm of Patankar (1980), for the continuous phase flow and accounting for the various coupling between the phases, in multiphase flows, by the principles of the IPSA (Spalding, 1983).

The finite volume approach

Since the pneumatic drying model can only be solved numerically, the values of the various model's variables can be obtained in discrete points of the computational domain. Hence, the numerical procedure includes discretization of the calculation domain into torus-shaped final volumes. In our developed model, a "staggered grid" was adopted. The various motivations for adoption of "staggered grid" can be found in Versteeg and Malalasekera (1998). The idea is to evaluate scalar variables, such as pressure, temperature, etc., at ordinary nodal points and to evaluate vector variables, such as the phase velocity, on staggered grids centered with the cell faces.

The implementation of the axisymmetric staggered gird is shown in Figure 2. The scalar variables are stored at the nodes marked (○). The velocities are defined at the cell faces in between the nodes and are indicated by arrows (⇒). The solid grid lines are numbered by means of capital letter. In the z-direction the numbering is $\ldots, I-1, I, I+1, \ldots$ etc., and the r-direction $\ldots, J-1, J, J+1, \ldots$ etc. Lower case letters denotes the dashed lines that construct the faces of the scalar cells $\ldots, i-1, i, i+1, \ldots$ and $\ldots, j-1, j, j+1, \ldots$ in the z- and r-direction, respectively. A subscript system based on these indexes was used to define the locations of grid nodes and cell faces. Scalar nodes are located at the intersection of two solid grid lines and are identified by two capital letters; e.g. point P in Figure 2 that is denoted by (I,J). The velocities are stored at lateral faces of a scalar finite control volume. These are located at the intersection of a dashed line defining a cell boundary and a solid grid line and are, therefore, defined by a combination of a lower and a capital case letters;, e.g. the w-face of the cell around point P is identified by (i,J).

Discretization of the gas phase conservation equations

The momentum conservation equation of the gas phase, in its integral form, can be expressed by

$$a_{i,J} u_{iJ} = \sum a_{\mathrm{nb}} u_{\mathrm{nb}} + (p_{I-1,J} - p_{I,J}) A_{i,J} + b_{i,J} \tag{29}$$

where $b_{i,J} = \bar{S}\Delta V$ is the momentum source term multiplied by the finite volume of the computed cell and $A_{i,j}$ is the (east or west) cell face area of finite volume.

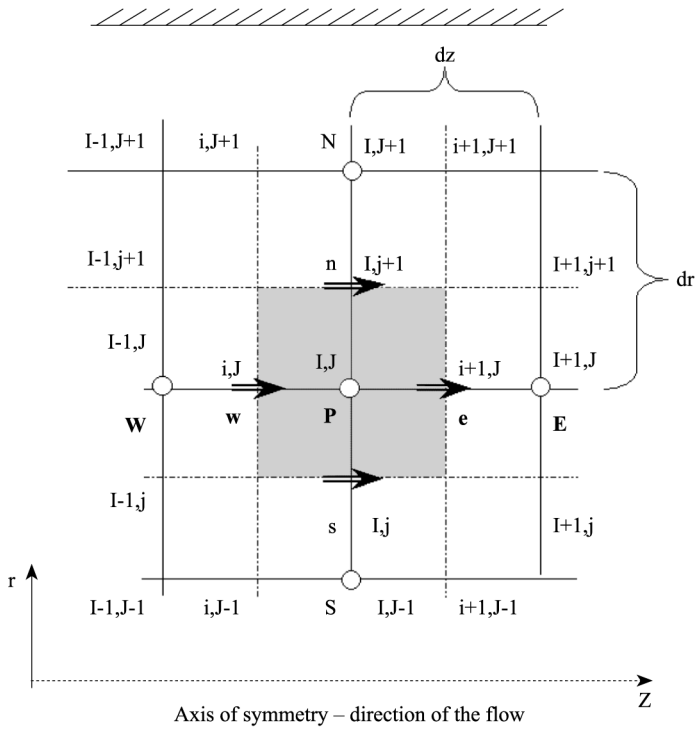

Figure 2.
The staggered grid

The pressure gradient source term has been discretized by means of a linear interpolation between the pressure nodes. The summation of $a_{\mathrm{nb}}u_{\mathrm{nb}}$ are calculated with the values of the neighbors cells, i.e. E, W, N and S, $(I-1, J)$, $(I+1, J)$, $(I, J+1)$ and $(I, J-1)$, respectively. The values of the coefficients $a_{i,J}u_{i,J}$ and $a_{nb}u_{nb}$ may be calculated by any type of the differencing methods (upwind, hybrid QUICK) that is suitable for convection-diffusion problems (Versteeg and Malalasekera, 1998). In the present study, a hybrid scheme (Spalding, 1972), which is based on a combination of central and upwind differencing schemes, was used. A second-order central differencing scheme was employed for small Peclet numbers ($\mathrm{Pe} < 2$) while a first-order upwind scheme was employed for large Peclet numbers ($\mathrm{Pe} \geq 2$). The hybrid-differencing scheme uses piecewise formulae based on the local Peclet number to evaluate the net flux through each control volume face. The Peclet number is evaluated at each face of the control volume. For example, the Peclet number at the west face is calculated by

$$\mathrm{Pe}_{\mathrm{w}} = \frac{F_{\mathrm{w}}}{D_{\mathrm{w}}} = \frac{(\rho u \phi)_{\mathrm{w}}}{\Gamma_{\mathrm{w}}/\delta z_{\mathrm{WP}}} \tag{30}$$

For two-dimensional flow the discretized form of a conservation equation for a scalar property, φ, can be written as

$$a_{\mathrm{P}}\varphi_{\mathrm{P}} = a_{\mathrm{W}}\varphi_{\mathrm{W}} + a_{\mathrm{E}}\varphi_{\mathrm{E}} + a_{\mathrm{S}}\varphi_{\mathrm{S}} + a_{\mathrm{N}}\varphi_{\mathrm{N}} \tag{31}$$

where the coefficients a_i of the property φ for the hybrid differencing scheme are presented in Table I. The hybrid difference scheme exploits the favorable properties of the upwind and central differencing schemes. The scheme is fully conservative and is unconditionally bounded. The scheme produces physically realistic solutions and is highly stable when compared with the higher order schemes. The disadvantage is that the accuracy in terms of Taylor series truncation error is only first-order (Versteeg and Malalasekera, 1998). The coefficients a_i contain combinations of the convective flux per unit mass, F, and the diffusive conductance, D, at cell faces (faces of the shaded control volume in Figure 2). Applying the new notation system the values of F and D for each of faces e, w, s and n of the control volume was written.

$$F_{\mathrm{w}} = (\rho u \phi)_{\mathrm{w}} = \frac{F_{i,J} + F_{i-1,J}}{2} = \frac{1}{2}\left[\left(\frac{\rho_{I,J}\phi_{I,J} + \rho_{I-1J}\phi_{I-1,J}}{2}\right)u_{i,J} + \left(\frac{\rho_{I-1,J}\phi_{I-1,J} + \rho_{I-2,J}\phi_{I-2,J}}{2}\right)u_{i-1,J}\right] \tag{32}$$

$$F_{\mathrm{e}} = (\rho u \phi)_{\mathrm{e}} = \frac{F_{i+1,J} + F_{i,J}}{2} = \frac{1}{2}\left[\left(\frac{\rho_{I+1,J}\phi_{I+1,J} + \rho_{I,J}\phi_{I,J}}{2}\right)u_{i+1,J} + \left(\frac{\rho_{I,J}\phi_{I,J} + \rho_{I-1,J}\phi_{I-1J}}{2}\right)u_{i,J}\right] \tag{33}$$

Based on the above mentioned assumption, there are no radial velocity components, and therefore,

$$F_{\mathrm{n}} = F_{\mathrm{s}} = 0 \tag{34}$$

$$D_{\mathrm{w}} = \frac{\Gamma_{I-1,J}}{dr}, \quad \text{for } dr = \text{const} \tag{35}$$

$$D_{\mathrm{e}} = \frac{\Gamma_{I,J}}{dr}, \quad \text{for } dr = \text{const} \tag{36}$$

$$D_{\mathrm{s}} = \frac{\Gamma_{I-1,J} + \Gamma_{I,J} + \Gamma_{I-1,J-1} + \Gamma_{I,J-1}}{4dz}, \quad \text{for } dz = \text{const} \tag{37}$$

$$D_{\mathrm{n}} = \frac{\Gamma_{I-1,J+1} + \Gamma_{I,J+1} + \Gamma_{I-1,J} + \Gamma_{I,J}}{4dz}, \quad \text{for } dz = \text{const} \tag{38}$$

Coefficients	Expression
a_{P}	$a_{\mathrm{P}} = a_{\mathrm{W}} + a_{\mathrm{E}} + a_{\mathrm{S}} + a_{\mathrm{N}} + \Delta F$
a_{W}	$\max\left[F_{\mathrm{w}}, \left(D_{\mathrm{w}} + \frac{F_{\mathrm{w}}}{2}\right), 0\right]$
a_{E}	$\max\left[-F_{\mathrm{e}}, \left(D_{\mathrm{e}} - \frac{F_{\mathrm{e}}}{2}\right), 0\right]$
a_{S}	$\max\left[F_{\mathrm{s}}, \left(D_{\mathrm{s}} + \frac{F_{\mathrm{s}}}{2}\right), 0\right]$
a_{N}	$\max\left[-F_{\mathrm{n}}, \left(D_{\mathrm{n}} - \frac{F_{\mathrm{n}}}{2}\right), 0\right]$
ΔF	$F_{\mathrm{e}} - F_{\mathrm{w}} + F_{\mathrm{n}} - F_{\mathrm{s}}$

Table I.
Coefficients of the general discretized form of a conservation equation for a scalar property, φ

Discretization of the solid phase conservation and other transport equations

The solid phase balance equations and other transport equations (equations (21), (22) and (24)), were obtained as a set of ordinary differential equations. The general form of these equations is

$$\frac{\mathrm{d}\varphi}{\mathrm{d}z} = f(\varphi) \tag{39}$$

The left side expression was evaluated by first-order forward difference approximation.

$$\frac{\mathrm{d}\varphi}{\mathrm{d}z} = \frac{\varphi(z_0 + \Delta z) - \varphi(z_0)}{\Delta z} \tag{40}$$

The solution algorithm

The developed solution algorithm, shown in Figure 3, is based on the SIMPLE algorithm for solving pressure-linked equations. Since the discrete form of the balance equations present the solution variables over the computational domain implicitly, prediction-correction procedure for calculating the pressure and the model's unknowns in the staggered grid was used. The couplings between the phases were considered by the principles of the IPSA.

The solution starts with initial guess of the pressure field p^*. Then the velocity field of the gas phase is obtain by solving the discretized momentum equation for gas phase (equation (29)), to obtain the gas phase velocity, u^* at the cells' interfaces.

$$a_{i,J}u^*_{i,J} = \sum a_{\mathrm{nb}}u_{\mathrm{nb}} + (p^*_{I-1,J} - p^*_{I,J})A_{i,J} + b_{i,J} \tag{41}$$

In order to correct the initial guess of the pressure field a correction pressure, p', was define by the difference between the correct pressure field p and the guessed pressure field p^*

$$p^* = p - p' \tag{42}$$

Similarly, velocity correction was defined as the difference between the correct velocity field u and the solution of the guessed gas phase velocity, u^*.

$$u^* = u - u' \tag{43}$$

Substitution of equations (41)-(43) into (29) together with some mathematical manipulations results in the equation for velocity correction.

$$a_{i,J}u'_{i,j} = \sum a_{\mathrm{nb}}u'_{\mathrm{nb}} + (p'_{I-1,J} - p'_{I,J})A_{i,J} \tag{44}$$

Now the well known approximation of the SIMPLE algorithm $\sum a_{\mathrm{nb}}u'_{\mathrm{nb}} \approx 0$ was adopted and equation (44) was simplified. Detailed explanation on this approximation can be found in Patankar (1980).

$$u'_{i,J} = d_{i,J}(p'_{I-1,J} - p'_{I,J}) \tag{45}$$

$$d_{i,J} = \frac{A_{i,J}}{a_{i,J}} \tag{46}$$

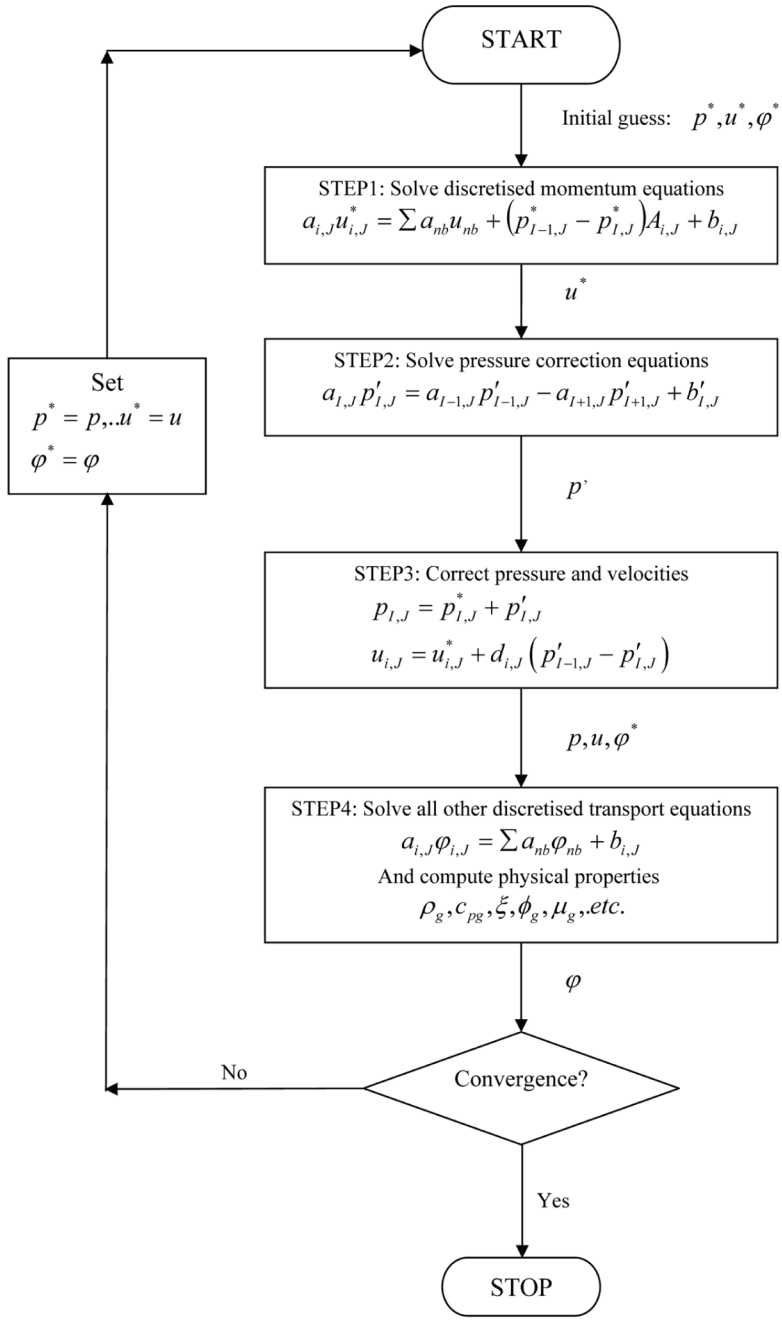

Figure 3.
Block diagram of the solution's algorithm

Finally, substitution of equation (45) back into the definition of the velocity correction yields to

$$u_{i,J} = u^*_{i,J} + d_{i,J}(p'_{I-1,J} - p'_{I,J}) \tag{47}$$

Solving the momentum equation does not satisfy the continuity. Hence, the next step of the algorithm is to solve the "pressure correction equation" that will satisfy the continuity equation of the gas phase.

$$(\rho\phi uA)_{i+1,J} - (\rho\phi uA)_{i,J} = S_{\mathrm{m}} \tag{48}$$

Substituting the solution of the gas velocity (equation (47)) into the continuity equation (equation (48)) results in

$$\begin{aligned} &\rho_{i+1,J}\phi_{i+1,J}A_{i+1,J}(u^*_{i+1,J} + d_{i+1,J}(p'_{I,J} - p'_{I+1,J})) \\ &\quad - \rho_{i,J}\phi_{i,J}A_{i,J}(u^*_{i,J} + d_{i,J}(p'_{I-1,J} - p'_{I,J})) = S_{\mathrm{m}} \end{aligned} \tag{49}$$

This may be rewritten to obtain the "pressure correction equation" for the two-fluid model as

$$\begin{aligned} [(\rho\phi dA)_{i+1,J} + (\rho\phi dA)_{i,J}]p'_{I,J} &= (\rho\phi dA)_{i+1,J}p'_{I+1,J} + (\rho\phi dA)_{i,J}p'_{I-1,J} \\ &\quad + [(\rho\phi u^*A)_{i,J} - (\rho\phi u^*A)_{i+1,J}] + S_{\mathrm{m}} \end{aligned} \tag{50}$$

or as

$$a_{I,J}p'_{I,J} = a_{I-1,J}p'_{I-1,J} - a_{I+1,J}p'_{I+1,J} + b'_{I,J} \tag{51}$$

where,

$$a_{I,J} = a_{I+1,J} + a_{I-1,J} \tag{52.1}$$

$$a_{I+1,J} = (\rho\phi dA)_{i+1,J} \tag{52.2}$$

$$a_{I-1,J} = (\rho\phi dA)_{i,J} \tag{52.3}$$

$$b'_{I,J} = (\rho\phi u^*A)_{i,J} - (\rho\phi u^*A)_{i+1,J} + S_{\mathrm{m}} \tag{52.4}$$

By solving the "pressure correction equation", the continuity is satisfied and the pressure correction field is obtained. Thus, the corrected pressure field can be obtained by using equation (42) and recalculating the velocity filed by resolving equation (47). The process of discretizing the governing equations of fluid flow, heat and mass transfer results in a system of linear algebraic equations. Generally, direct and indirect methods can be used for solving linear algebraic equations. For a large set of equations an indirect iterative method is preferred. In this study, the tri-diagonal matrix algorithm (TDMA) was adopted for solving the algebraic set of equations. This method is widely applied in CFD programs and it solves the equations iteratively, in line-by-line fashion. Detailed explanation concerning this technique can be found in Versteeg and Malalasekera (1998). After evaluating gas phase pressure and velocity fields, the rest of the discretized transport equation for the gas phase and the dispersed phase were solved and their characteristics' fields were obtained. The convergences of the various properties were analyzed and the iteration starts again if the solution was not converged.

Boundary condition

The boundaries of a pneumatic dryer include inlet, outlet and wall. In the present study, it was assumed that the flow is aximertic with respect to the dryer center. Hence, four types of boundary conditions were implemented, i.e. inlet, outlet, wall and symmetry. The implementations of these boundary conditions are shown in Figure 4. As can be seen, the grid was extended to store the values of the physical properties at the boundaries. The boundary conditions applied in the discretized equation via source term. It should be noted that only inlet boundary conditions are needed for solving the unknowns that were considered via ordinary differential equations, i.e. dispersed phase velocity, temperature, particles' size diameter, etc. However, the influences on these unknowns from the other boundaries were reflected via the interactions between the phases.

Inlet boundary conditions. The distributions of all flow variables, except pressure, were specified at the inlet to the pneumatic dryer. The flow direction was assumed to be from the left to the right (Figure 4). Uniform inlet conditions were assumed.

Outlet boundary conditions. When the location of the outlet is far enough from the inlet, the flow reaches a fully developed state where no change occurs in the flow direction. At this boundary zero gradients for all variables, except pressure, in the flow direction ($\partial/\partial z = 0$) were assumed. Additional grid line $I = NI + 1$ was imposed at the outlet boundary conditions (Figure 4) and the values of the variables at the outlet were substituted as flows.

$$\varphi_{NI+1,J} = \varphi_{NI,J} \tag{53}$$

During the iteration cycles there is no guarantee that the normal velocities will conserve mass over the computational domain as a whole. To ensure that overall continuity is satisfied, i.e. the mass flux going out of the domain (M_{out}) is equal to that entering into the domain (M_{in}), the outlet velocity was calculated by

$$u_{NI+1,J} = u_{NI,J} \times \frac{M_{\text{in}}}{M_{\text{out}}} \tag{54}$$

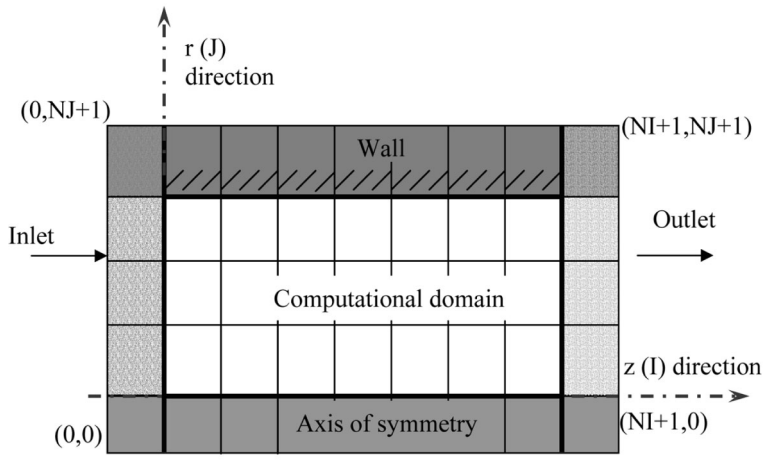

Figure 4.
Mapping additional cells for implantation boundary condition

The pressure field obtained by solving the pressure correction equation does not give absolute pressure (Patankar, 1980), therefore a reference value of normal atmospheric pressure for the absolute pressure was specified at the dryer outlet.

Wall boundary conditions. During this study, non-slip and non-penetrating wall conditions were assumed. Therefore, the gas phase velocity in the additional grid line was set to be zero ($J = NJ + 1$, the grid line used for implementation wall boundary conditions). Since there is no mass transfer of water through the pipeline wall, the gradient of the water moisture content was set to zero, $(\partial X_{\mathrm{w}}/\partial r|_{r=R} = 0)$. This was implemented by setting the values of the water moisture content at the wall as the near by cells, i.e. $X_{I,J+1} = X_{I,J}$.

Four types of boundary conditions are often being set for the gas phase temperature in pneumatic dryers. These types are listed below.

- Constant wall temperature ($T_{\mathrm{wall}} = \mathrm{const}$).
- Known temperature profile ($T_{\mathrm{wall}} = T(z)$).
- Constant heat flax ($\partial T/\partial r = \mathrm{const}$).
- Adiabatic wall condition ($\partial T/\partial r = 0$).

All these types of temperature wall condition were successfully implemented in the developed numerical model and used during the investigation of real drying processes.

Symmetry boundary condition. The conditions at a symmetry boundary are no flow or scalar flux across the boundary. Hence, the derivative of every properties at the axis of symmetry was set to zero, $(\partial \varphi/\partial r|_{r=0} = 0)$. This was implemented by setting the values at the axis of symmetry as the near by cells, i.e. $\varphi_{I,0} = \varphi_{I,1}$

Solution quality and validation

Usually a successful numerical algorithm should follow three mathematical concepts: convergence, consistence and stability. Patankar (1980) formulated three new rules, namely, conservativeness, boundedness and transportiveness, that are embedded into the final volume scheme and are commonly accepted an alternatives for the rigorous mathematical concepts of convergence, consistence and stability. In the present study, the convergence of the numerical predictions were analyzed by two means. The first was by reducing the control volume size and checking that the difference between the results of the two simulations is negligibly small. Then the predictions of the numerical simulations were compared with independent experimental data. The consistency of the finite volume scheme is well known since the formulation of the discrete balance equations of every control volume is equivalent to the formulation of the differential balance equations. To assure solution stability under-relaxation technique was used. This technique restrains undesirable oscillations, which can occur during the iterative solution procedure. A correct choice of under-relaxation factors is essential for cost-effective simulations. Too large values may lead to oscillatory or even divergent iterative solutions and a value, which is too small, will cause extremely slow convergence. Unfortunately, the optimum values of under-relaxation factors were flow dependent and must be found on a case-by-case basis.

In order to validate the theoretical and the numerical models, the predictions of the numerical simulations were compared with experimental data. The pneumatic drying model was solved numerically for two drying processes, i.e. drying of PVC and sand

particles. Comparison between the results of the two-dimensional model and the results of other one-dimensional models and experimental data require a representation model for presenting the two-dimensional results in "one-dimensional" manner. An average technique was used to obtain the average values of the various solution properties in the dryer cross section. The average value of any property, φ, (except the temperature) in the dryer cross sectional area was obtained by "mass weighted" method as follows.

$$\varphi = \frac{2\pi \int_0^R \rho u \varphi r \, \mathrm{d}r}{2\pi \int_0^R \rho u r \, \mathrm{d}r} \tag{55}$$

The average temperature of each phase was evaluated by the mean bulk temperature, or energy average fluid temperature across the tube.

$$T_{\mathrm{ave}} = \frac{2\pi \int_0^R \rho u c_p T r \, \mathrm{d}r}{2\pi \int_0^R \rho u c_p r \, \mathrm{d}r} \tag{56}$$

The first validation was done by comparison between the predications of the numerical simulations and the experimental results of Baeyens *et al.* (1995) that were obtained in a 1.25 m diameter and 25 m long pneumatic dryer. In this study, 180 μm PVC particles having density of 1195 kg/m^3 and mass flow rate of 10.52 kg/s were dried with 1.51 kg/s air mass flow rate. Comparison between the predictions of the numerical simulations and the experimental data for changes of air temperature and particle moisture content with dryer length under known wall's temperature conditions is presented in Figure 5(a) and (b), respectively. During this study the computational grid was made of 2000×50 cells and it was assumed that in average the pipe wall temperature is just about the outlet air temperature, as presented by Baeyens *et al.* (1995), and it is falling linearly from 325 K at the inlet to 320 K at the outlet. In these figures, the solid symbols represent the experimental data that were published by Baeyens *et al.* (1995) and the two curves represent the predictions of the numerical simulations (present paper and Levy and Borde, 1999). It is clearly seen that the numerical model predicted the temperature profile (Figure 5(a)) very well while the predictions of the numerical simulations for the particle moisture content (Figure 5(b)) were fairly good. From these figures, it can also be seen that the heat and the mass transfer rates during the second drying period (i.e. the curves gradient at low moisture contents) was predicted very well.

The predictions of the numerical simulations for the drying of sand particles in a laboratory scale pneumatic dryer were also compared with the experimental results of Rocha (1988) (presented by Silva and Correa (1998)). The computational grid was made of 1828×12 cells. 380 μm sand particles having density of 2622 kg/m^3 and solid mass flow rate of 4.74×10^{-3} kg/s were dried with 3.947×10^{-2} kg/s air mass flow rate in a 4 m high pneumatic dryer with diameter of 5.25 cm. Comparison between the predictions of the numerical simulations and the experimental data for changes of gas temperature, solid temperature, gas humidity and particle's moisture content with length under known wall temperature operating conditions is presented in Figure 6(a)-(d), respectively. For this case it was assumed that in average the pipe wall temperature is just about the outlet air temperature and it is falling linearly

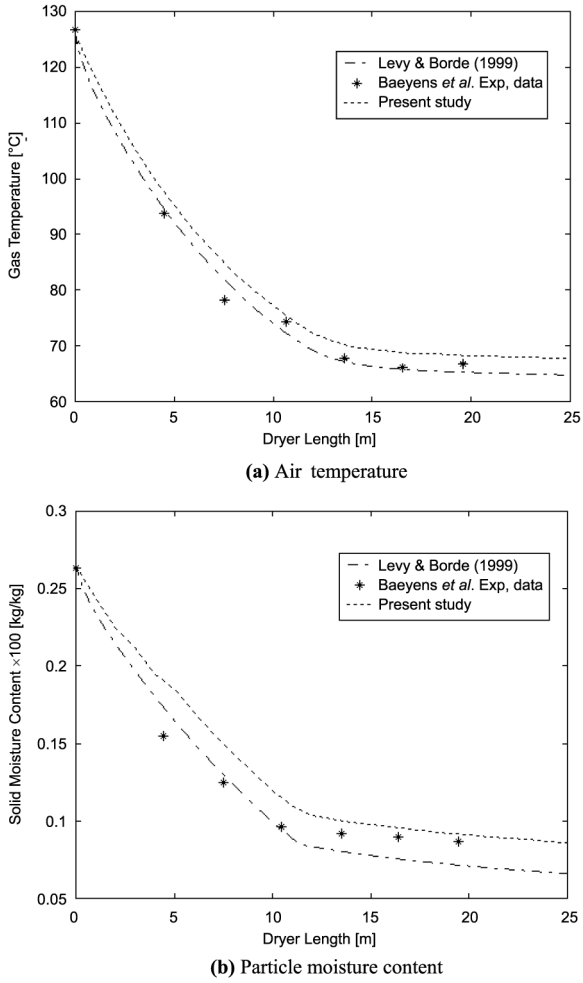

Note: Levy & Borde (1999) model and the experimental data for drying of 180 m PVC particles with 10.52 kg/s and 1.51 kg/s air and particles mass flow rates, respectively, and for a known pipe wall's temperature flow conditions

Figure 5.
Comparison between the predictions of the numerical simulations. (a) air temperature and (b) particle moisture content

from 360 K at the inlet to 354 K at the outlet. In these figures, the star symbols represent the experimental data of Rocha (1988) that were presented by Silva and Correa (1998) and the other curves and symbols represent the predictions of various models and numerical simulations. From these figures it can be seen that the predictions of the two-dimensional numerical simulations fit fairly well with the experimental data and both one-dimensional DryPak (Pakowski, 1996) and Levy and Borde (1999) models.

Since the theoretical pneumatic drying model and the numerical simulations done in the course of this study predicated successfully the most important flow parameters

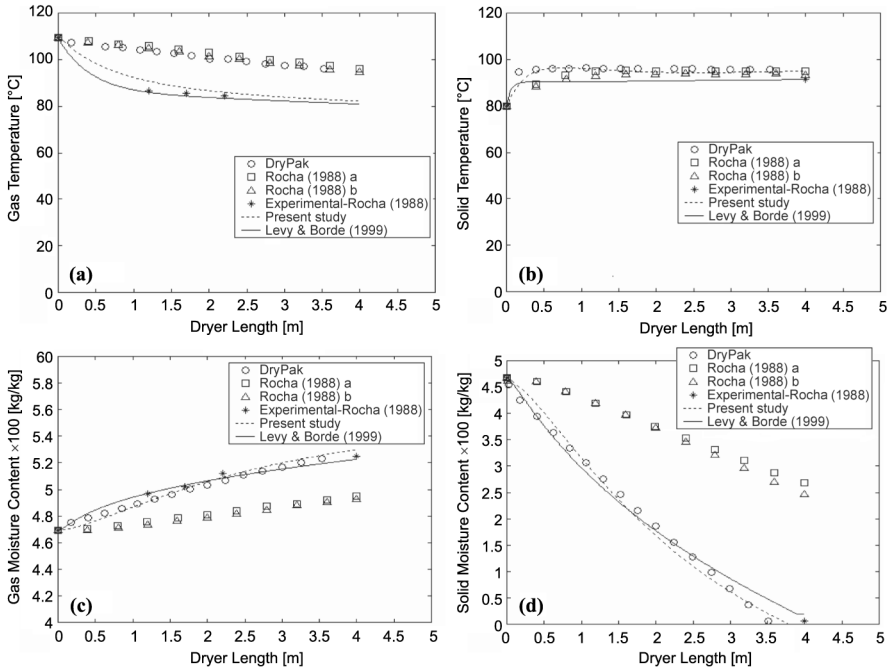

Figure 6.
Comparison between the numerical predictions

Note: DryPak model, Rocha (1988) and Levy & Borde (1999) models and the experimental data for changes of (a) gas temperature, (b) solid temperature, (c) gas humidity and (d) particle's moisture content with length under known wall temperature operating conditions

(gas temperature, solid temperature, gas humidity and particle's moisture content) of the drying process it was concluded that the presented model can be used for further investigations.

Two-dimensional representation of the flow field

Due to the lack of two-dimensional experimental data (i.e. radial distribution), the predictions of the numerical simulations for two-dimensional characteristics distributions could not be validated. Based on the reliable one-dimensional validation of the theoretical and the numerical models, it was decided to investigate the two-dimensional distributions of the flow characteristics. In contrast to one-dimensional simulation, two-dimensional simulations provide much more information about the behavior of flow properties in every point of axisymmetry computational domain.

In order to investigate the capability of the theoretical and numerical models, the predictions of the numerical simulations for the drying of 380 μm sand particles in the 4 m high pneumatic dryer with a diameter of 5.25 cm were adopted. The radial distributions of the dispersed phase and the gas phase velocities, particles and gas moisture contents and gas phase temperature after 1, 2, 3 and 4 m from the pipeline inlet are presented in Figure 7(a)-(e), respectively. As can be seen the radial distribution of phases' velocities result in uneven cross sectional particles' concentration and moisture

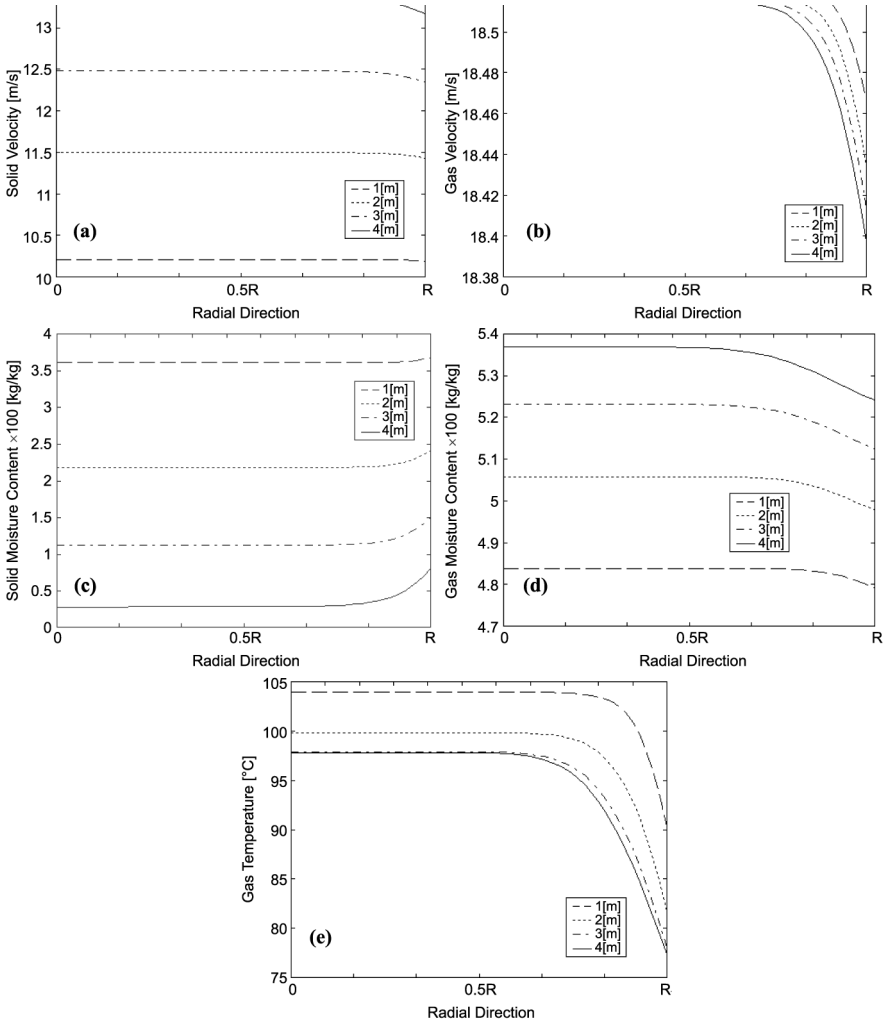

Note: (a) dispersed phase velocity, (b) gas phase velocity, (c) particle's moisture content (d) gas moisture, and (e) gas phase temperature field after 1, 2, 3, and 4m from the pipeline inlet

Figure 7.
Radial distribution

content. Hence, special care should be placed in order to ensure the demand that all the particles will have the required moisture content at the pneumatic dryer exit.

The formation of various boundary layers for both phases can be seen clearly (Figure 7). A significant temperature difference between the central dryer region and near wall region is evident. This is emphasized at the fully developed area which was achieved about 3 m from the dryer inlet. The temperature differences in cross section of the dryer cause radial particle's moisture content distribution (Figure 7(c)). As can be seen, solid particles at the proximity of the wall have higher moisture than in the dryer central area. It should be mentioned that the lower velocities of both phases in the

vicinity of the dryer wall also contribute to the lower heat and mass transfer between the phases. In order to increase the heat and mass transfer at the boundary layer, the wall's temperature might be controlled by heating the dryer walls. Thus, the developed model may provide a design tool for predicting the required wall temperature. The gas moisture content, shown in Figure 7(d), is characterized by more homogeneous distribution due to vapor diffusion in carrier gas.

Generally, the state of the dispersed phase at the dryer outlet is more significant than that of the drying gas, since the particulate materials is the target product of drying process. Properties variation may damage the final product quality. Therefore, this type of numerical investigation may serve as a design tool in order to maximize the products quality.

Conclusions

A finite volume approach for solving two-dimensional, two-fluids flows with heat and mass transfer was developed for predicting the flow of wet particulate materials through a pneumatic dryer. The model was solved for a two-dimensional axisymmetric steady-state condition and considering axial and radial profiles for the flow variables. A two-stage drying process was implemented. The predictions of the numerical simulations were validated for two cases: drying process of wet PVC particles in a large-scale pneumatic dryer and to the drying process of wet sand in a laboratory-scale pneumatic dryer. The predictions of the numerical solutions were also compared with the results of other numerical investigations. The successful comparisons validate the theoretical and the numerical models. Radial distributions of the flow characteristics were examined. The existence of boundary layers along the pipeline walls were presented. Further investigations are needed in order to validate the two-dimensional distribution of the flow characteristic.

References

Abuaf, N. and Staub, F.W. (1987), "Drying of liquid-solid slurry droplets, Drying'86", *Proceedings of the 5th International Drying Symposium*, Vol. 1, pp. 227-48.

Andrieu, J. and Bressat, R. (1982), "Experimental and theoretical study of a pneumatic dryer", *Proceedings of the 3rd International Drying Symposium*, Vol. 2, pp. 10-19.

Baeyens, J., van Gauwbergen, D. and Vinckier, I. (1995), "Pneumatic drying: the use of large-scale experimental data in a design procedure", *Powder Technol.*, Vol. 83, pp. 139-48.

Bowen, R.M. (1976) in Eringen, A.C. (Ed.), *Theory of Mixtures in Continuum Physics*, Academic Press, New York, NY, pp. 1-127.

Clift, R., Grace, J. and Weber, M.E. (1987), *Bubbles, Drops and Particles*, Academic Press, New York, NY.

Crowe, C.T. (1982), "REVIEW – numerical models for dilute gas-particle flows", Transactions of the ASME", *J. Fluids Eng.*, Vol. 104, pp. 297-311.

Cundall, P.A. and Strack, O.D. (1979), "A discrete numerical model for granular assemblies", *Geotechnique*, Vol. 29, pp. 47-65.

Gidaspow, D. (1994), "Multiphase", *Flow and Fluidization*, Academic Press, Boston, MA.

Levi-Hevroni, D., Levy, A. and Borde, I. (1995), "Mathematical modelling of drying of liquid/solid slurries in steady sate one dimensional flow", *Drying Technol.*, Vol. 13 Nos 5/7, pp. 1187-201.

Levy, A. and Borde, I. (1999), "Steady-state one-dimensional flow for a pneumatic dryer", *Chen. Eng. & Proc.*, Vol. 38, pp. 121-30.

Levy, A., Mason, D.J., Borde, I. and Levi-Hevroni, D. (1988), "Drying of wet solids particles in a steady-state one-dimensional flow", *Powder Technol.*, Vol. 85, pp. 15-23.

Mindziul, Z. and Kmiec, A. (1996), "Modeling gas-solid flow in a pneumatic-flash dryer, Drying'96", *Proceedings of the 10th International Drying Symposium*, Vol. A, pp. 275-82.

Pakowski, Z. (1996), DryPak v.3, Program for psychometric and drying computation.

Patankar, S.V. (1980), *Numerical Heat Transfer and Fluid Flow*, Hemisphere Publishing Corporation, New York, NY.

Rocha, S.C.S. (1988), "Contribution to the study of pneumatic drying: simulation and influence of the gas-particle heat transfer coefficient", PhD Thesis (in Portuguese), São Paulo University, São Paulo.

Rocha, S.C.S. and Paixão, A.E.A. (1996), "Pseudo two-dimensional model for a pneumatic dryer, Drying'96", *Proceedings of the 10th International Drying Symposium*, Vol. A, pp. 340-8.

Silva, M.A. and Correa, J.L.G. (1998), "Using DryPak to simulate drying process, Drying'98", *Proceedings of the 11th International Drying Symposium*, Vol. A, pp. 303-10.

Skuratovsky, I., Levy, A. and Borde, I. (2003), "Two-fluid, two-dimensional model for pneumatic drying", *Drying Technology*, Vol. 21 No. 9, pp. 1649-72.

Spalding, D.B. (1972), "A novel finite-difference formulation for differential expressions involving both first and second derivatives", *Int. J. Numer. Methods Eng.*, Vol. 4, p. 551.

Spalding, D.B. (1983), "Developments in the IPSA procedure for numerical computation of multiphase-flow phenomena with interphase slip, unequal temperatures, etc.", *Numerical Properties and Methodologies in Heat Transfer*, Hemisphere, Washington, DC, pp. 421-76.

Versteeg, H.K. and Malalasekera, W. (1998), *An Introduction to Computational Fluid Dynamics, The Finite Volume Method*, Longman Group Ltd, London.